J Electroceram (2008) 20:81–87
DOI 10.1007/s10832-007-9357-2

Structural and ferroelectric characterization of BMZ–BF–PT ceramics

Seema Sharma · D. A. Hall

Received: 14 February 2006 / Accepted: 22 October 2007 / Published online: 9 November 2007

Abstract Bismuth containing crystalline solid solutions of $[(BiMgZrO_3)_{1-y}$–$(BiFeO_3)_y]_x$–$(PbTiO_3)_{1-x}$, (BMZ–BF–PT) have been synthesized by high temperature solid-state reaction technique. The crystalline symmetry varied with the composition, indicating good solid state solubility of BMZ and BF with PT. X-ray diffraction (XRD) reveals that BMZ–PT and BMZ–BF–PT have a single-phase perovskite structure. The MPB of BMZ–PT lies in the region x=0.55 to x=0.6, which is supported by the transformation from rhombohedral to tetragonal phase. The SEM photographs exhibit the uniform distribution of grains in the matrix. Polarization–electric field hysteresis studies were carried out at Room Temperature for all the compositions up to an applied electric field of 3.5 kV/mm. It was found that with the increase of $BiFeO_3$ content in the composition the remnant polarization decreases and the ferroelectric loops get constricted. Variation of dielectric constant with temperature shows that there is an increase in Transition temperature (T_C) with the increase in applied frequency indicating a relaxor characteristic of the compound. Our results show that BMZ–BF–PT is a good low-lead (Pb) high-temperature ferroelectric ceramic.

Keywords X-Ray diffraction · Perovskite · Ferroelectric · Hysteresis

S. Sharma (✉)
Department of Physics,
Birla Institute of Technology and Science—Goa Campus,
Goa 403726, India
e-mail: seema_sharma26@yahoo.com

D. A. Hall
Materials Science Center, School of Materials,
University of Manchester,
Manchester M1 7HS, UK

1 Introduction

Piezoelectric ceramics based on the perovskite Lead zirconate titanate (PZT) system are widely used as sensors and actuators. Traditional applications of these materials include underwater sonar, ultrasound transducers and actuators. Advances in electronics and computer control have also led to the incorporation of piezoelectric materials into common devices and smart systems [1, 2]. There are a number of piezoelectric sensors and devices in automotive, aerospace and related industrial applications often in vibration sensing and/or cancelling systems. Both the automotive and aerospace industries have expressed the need for actuation and sensing at higher temperatures Specifically, under-hood automotive applications such as internal vibration sensors, control surfaces, or active fuel injection nozzles require operation temperatures as high as 300 °C [3, 4]. Commercially available piezoelectric materials are generally limited to operating temperatures of one half transition temperature T_C or approximately 150 °C for most PZT formulations.

Perovskite PZT has come to dominate the world market for piezoelectric materials since its discovery in the mid 1950s. PZT based materials take advantage of a nearly temperature independent compositional phase boundary (Morphotropic phase boundary or MPB) between rhombohedral and tetragonal phases. The existence of these two thermodynamically equivalent phases leads to production of a highly domain oriented material during the required poling process, exhibiting enhanced dielectric and piezoelectric activity [1, 5].

Recently new high temperature ferroelectric materials based on $(1-x)$ $BiMeO_3$–x-$PbTiO_3$ solid solutions (where Me^{3+}=Sc, In, Fe, In, Yb, etc) have been identified [6–8] exhibiting enhanced piezoelectric properties in relation to

PZT. Guided by a perovskite tolerance factor relationship with T_C, low tolerance factor $BiMeO_3$ systems have projected transition temperature greater than PZT. $BiScO_3$–$PbTiO_3$ (BS–PT) exhibits an MPB at 64% $PbTiO_3$ between an untilted rhombohedral (R3m) and a tetragonal phase (P4mm) phase [9] with a Transition temperature ~450 °C [7]. The disadvantage of this material is the high cost of Sc_2O_3 which means that the production of BS–PT ceramics is not economically viable. $BiFeO_3$–$PbTiO_3$ (BF–PT) exhibits an MPB at 30% of $PbTiO_3$ between a tilted rhombohedral (R3c) and a tetragonal phase (P4mm) phase [10]. Several studies report that the MPB composition has a high T_c (650 °C), but to date high ferroelectric/piezoelectric measurements have proven to be difficult, possibly due to the usually large c/a ratio (1.17) in the tetragonal phase close to the MPB and/or its high conductivity [11–13].

Since the high cost of BS–PT prohibits its commercial usage, a substitute for Sc_2O_3 is required. Previous solid solutions which have attempted to reproduce the properties of BS–PT, have either limited solid solubility or inferior properties, e.g. $BiInO_3$–PT [8], $BiGaO_3$–PT [13] and $BiMnO_3$–PT [14], $BiMg_{1/2}Ti_{1/2}O_3$–PT [15]. Here, therefore, Fe_2O_3 has been used as a partial substituent for Sc_2O_3.

Solid solution of $BiMgZrO_3$–$PbTiO_3$ (BMZ–PT) exhibits a stable perovskite structure. The objective of this article is to interpret the structure-property relations in a new ceramic system [$(1-x)$ $BiMgZrO_3$–$xPbTiO_3$] where x=0.65, 0.60, 0.55 and 0.50. In addition to this, the effect of addition of $BiFeO_3$ (BF) on structural and ferroelectric properties of $(1-x)$ BMZ–x PT (x=0.60), binary system has been investigated in this paper.

2 Experimental procedure

Polycrystalline samples of BMZ–PT (BMZ=35/40/45/50%, PT=65/60/55/50%) designated as 35–65, 40–60, 45–55, 50–50 and BMZ–BF–PT (BMZ=40%, BF=0/25/50% and PT=60%) designated as 40–0–60, 40–25–60 and 40–50–60, were prepared by high temperature solid state reaction technique. PbO, MgO, TiO_2, Bi_2O_3, Fe_2O_3 and ZrO_2 (all Aldrich AR grade) were used as the starting materials. Stoichiometric weights of MgO, PbO, TiO_2, Bi_2O_3, ZrO_2 and Fe_2O_3 were mixed and ball milled with distilled water for 48 h, using calcia stabilized zirconia balls as the grinding media. After drying in vacuum by using lyophilizer, calcination was carried out at 800 °C for 2 h in air followed by ball milling and drying. A single-phase formation was confirmed by the X-ray diffraction (XRD) technique. The calcined powder was pressed at 100 MPa to form cylindrical pellets using a cold isostatic press (CIP). The pellet was then sintered at 1050 °C for 1.5 h. A PbO rich atmosphere was maintained by placing $PbZrO_3$ powder in an alumina boat near the test samples in closed crucible configurations in order to minimize the lead loss during sintering.

XRD analysis was performed on a PW 3710 Philips diffractometer using CuK_α (λ=0.15405 nm) radiation in the

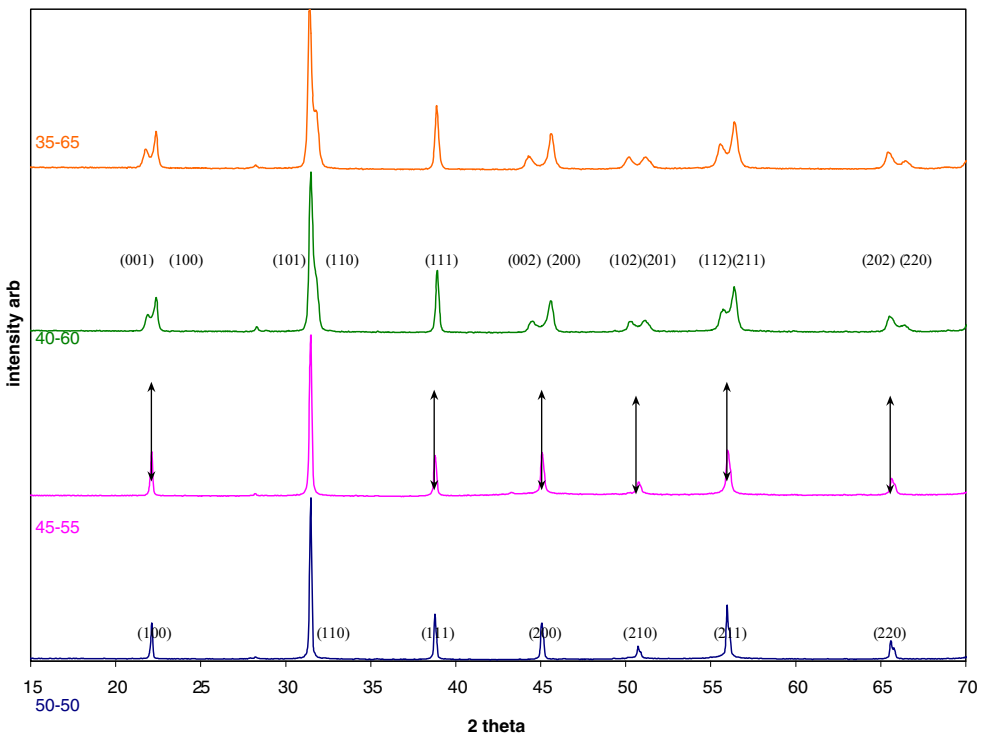

Fig. 1 XRD patterns of BMZ–PT (35–65, 40–60, 45–55 and 50–50) samples sintered at 1050 °C

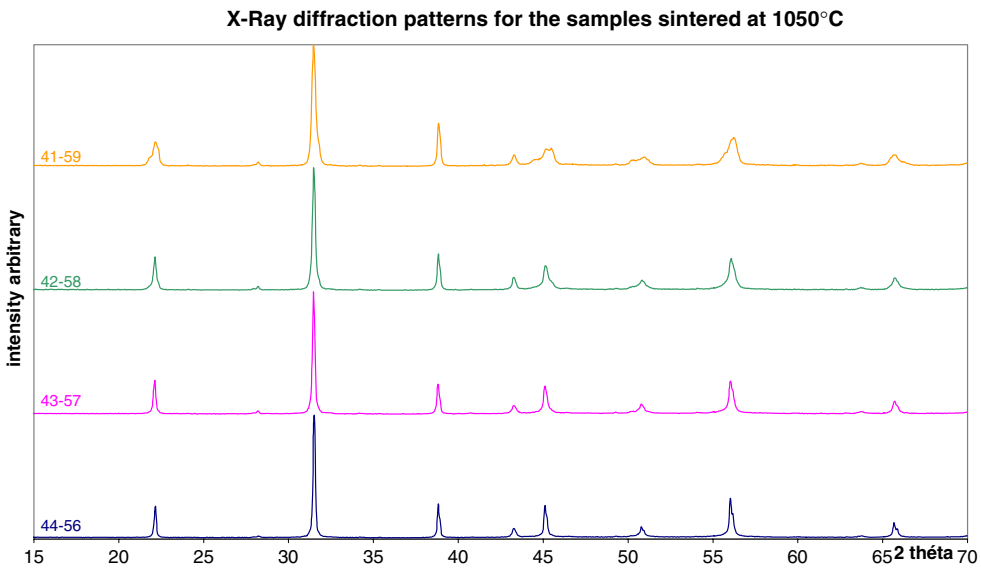

Fig. 2 XRD patterns of BMZ–PT (41–59, 42–58, 43–57 and 44–56) samples sintered at 1050 °C

range of 10°–80° to examine the phases present in the system. Analysis of the diffraction patterns was conducted using Celref V3 and XFIT software. Sintered pellets were polished to a 1 μm finish and thermally etched for 30 min at a temperature 100 °C below the sintering temperature. Polished surface microstructure was examined by scanning electron microscopy (SEM) (XL30FEG-Philips).

For electrical characterisation, the sintered pellets were polished to obtain smooth parallel faces. The polished pellets were electroded using a post fire silver paste (Dupont 6160), fired on at 850 °C. Dielectric permittivity (ε') and dielectric loss (ε'') were measured at the frequencies 0.1 kHz, 1, 10 and 100 kHz as a function of temperature (room temperature to 500 °C) by HP 4284A LCR Meter.

High field measurements were conducted at room temperature (22±2 °C) under silicon oil using a computer controlled function generator (HP 33120A) and a high voltage amplifier (Trek 609D-6). A current amplifier (Stanford research systems Model SR570) was used to measure the induced current, which was then integrated numerically to yield the charge Q and hence the polarisation P. The applied field and induced current waveforms were downloaded to the PC using a Tektronix TDS 420 DSO. Further details of the measurement method have been given in an earlier publication [16].The measurements were carried out using a 'burst-mode' waveform comprising two complete sinusoidal cycles. This procedure was used in preference to a continuous waveform in order to avoid field forced deageing effects [17].

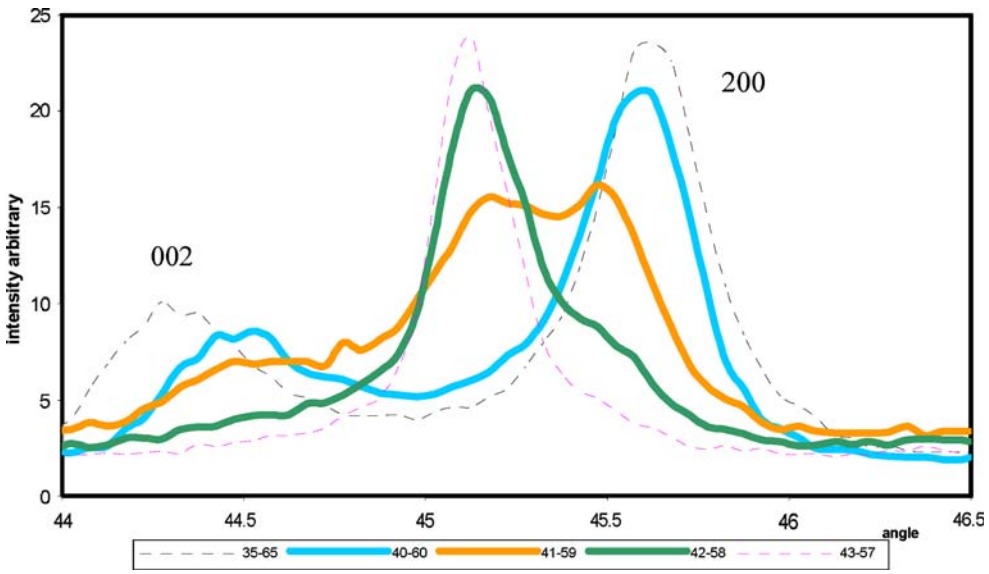

Fig. 3 High energy X-ray diffraction spectra of the sintered BMZ–PT compositions showing {200} reflections

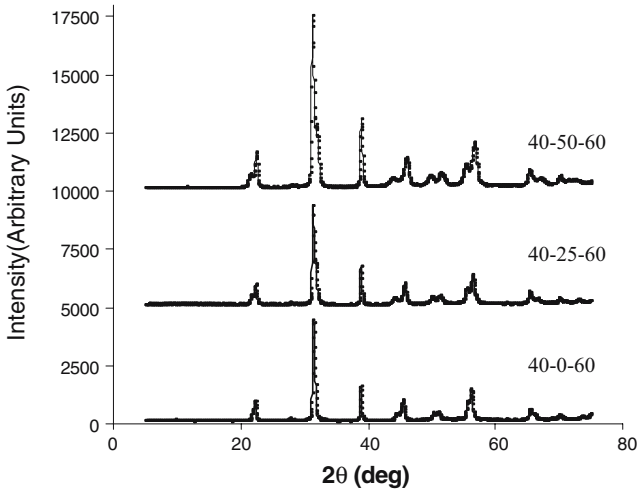

Fig. 4 Room temperature XRD pattern of BMZ–BF–PT samples

3 Results and discussion

3.1 XRD analysis

Figure 1 shows the room temperature XRD patterns of BMZ–PT (35–65, 40–60, 45–55 and 50–50) samples sintered at 1050 °C. The peaks in the XRD patterns were found to be sharp with distinct diffraction peaks.

A change of structure from rhombohedral to tetragonal between 45–55 and 40–60 compositions is evident from the XRD patterns. Hence, it is inferred from this that MPB lies between these two compositions [7]. This is also shown in Fig. 2 for the four specific BMZ–PT (41–49, 42–58, 43–57 and 44–56) compositions.

Higher PT content BMZ–PT (44–56) composition exhibit splitting of the {200} reflection into clearly separated $\{002\}_T$ and $\{200\}_T$ diffraction peaks. This effect can be seen more clearly in the XRD spectra as shown in Fig. 3 (zoom between 2θ=45–46.5°). A very small peak which appears almost on all the graphs at 2θ=43° (Fig. 2) corresponds probably to a TiO_2 rich second phase.

Figure 4 shows XRD patterns of BMZ–BF–PT (40–0–60, 40–25–60 and 40–50–60) samples sintered at 1050 °C. All XRDs show a pure perovskite phase with tetragonal structure.

The diffraction lines for the system [BMZ–BF–PT (BMZ=40%, BF=0/25/50% and PT=60%)] were indexed in different crystal systems and unit cell configurations using a computer programme package XFIT and CELREF. Standard deviations, $\Sigma\Delta d = d_{obs} - d_{cal}$ where d is the inter-planar spacing, were found to be minimum for tetragonal structure. The unit cell parameters and the tetragonality for the system with different $BiFeO_3$ content is shown in Table 1.

The splitting of (200), (210) and (211) peaks broaden with increase in BF content. The tetragonality is increasing with increase in $BiFeO_3$ in the sample. There is a 1.35% increase in tetragonality from 40–0–60 composition to 40–25–60 composition and another 1.34% increase from the 40–25–60 to 40–50–60 composition. This confirms the hardening effect of the inclusion of Fe content in the BMZ–PT system.

3.2 SEM analysis

Figure 5(a–c) shows SEM photographs of the fracture surfaces of 40–0–60, 40–25–60 and 40–50–60 compositions respectively.

The photographs show uniform grain size distribution. There is no preferred growth orientation and little porosity is observed. The black areas are pores and the thin white filaments are a liquid phase of $PbO–Bi_2O_3$ that appeared during sintering and is situated at the grain boundary region. The liquid phase is in fact an amorphous phase resulting from sintering. Referring to the binary phase

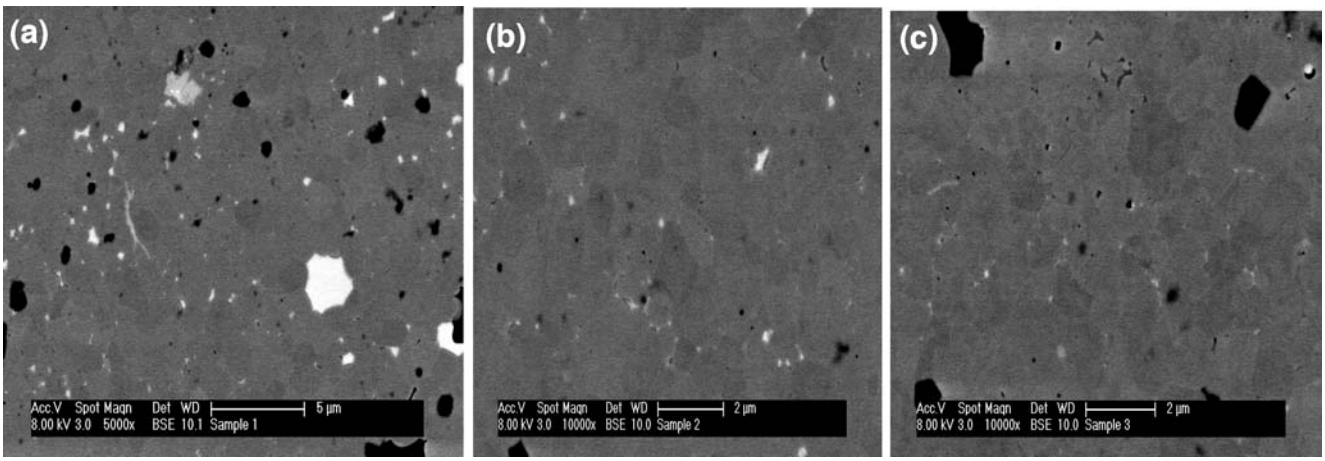

Fig. 5 (**a**) 40–0–60, polished surface, (**b**) 40–25–60, polished surface, (**c**) 40–50–60, polished surface, backscattered electron image backscattered electron image backscattered electron image

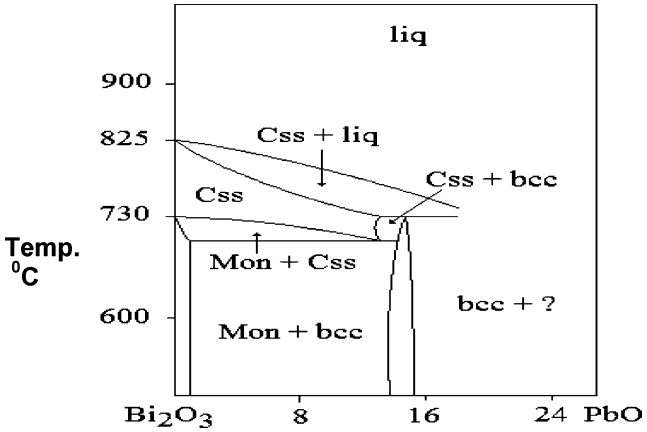

Fig. 6 Phase diagram of PbO–$B_{i2}O_1$

diagram (Fig. 6) of the PbO– Bi_2O_3 system, we can see that at the sintering temperature (i.e. 1000 and 1050 °C), the present phase is a liquid phase. And because the phase did not have time to recrystallize, this solidified as a glassy phase. The average grain size of all the compositions was found to be in the range from 1.5 to 2 μm.

The density of all the compositions obtained by Archemedes's principle was found to be greater than 95%.

Table 1 Unit cell parameters.

BMZ–BF–PT	$c/^0A$	$a/^0A$	Tetragonality=c/a
40–0–60	2.0131	1.9954	1.0179
40–25–60	2.0479	1.9854	1.0314
40–50–60	2.0621	1.9724	1.0454

3.3 Hysteresis analysis

Figure 7(a–c) shows the Polarization–electric field (P–E) hysteresis loops of all the compositions at different temperatures (RT-room temperature, 50, 100 and 150 °C) respectively. P–E loops of the samples show a gradual

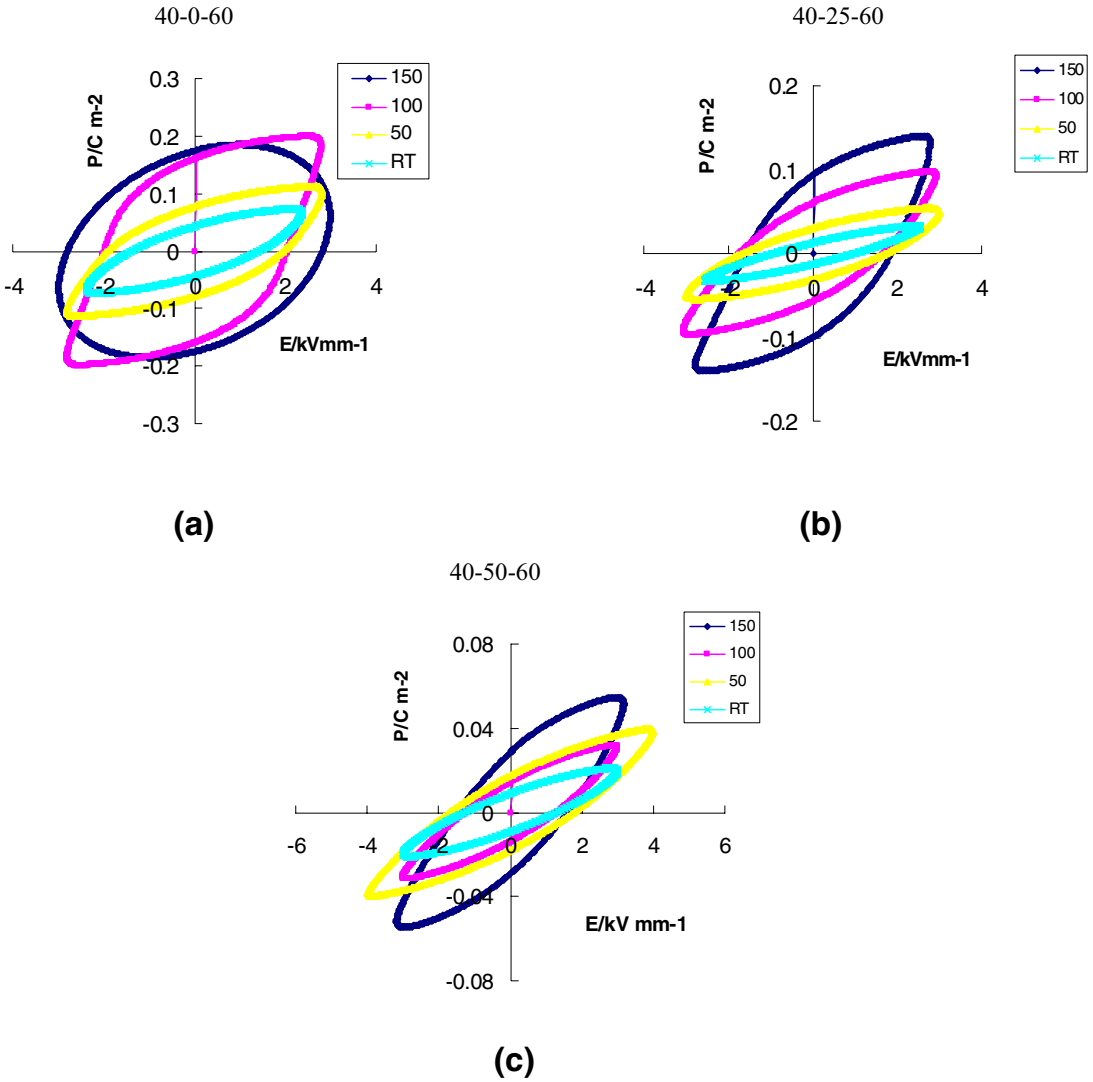

Fig. 7 P–E hysteresis loops of BMZ–BF–PT ceramics

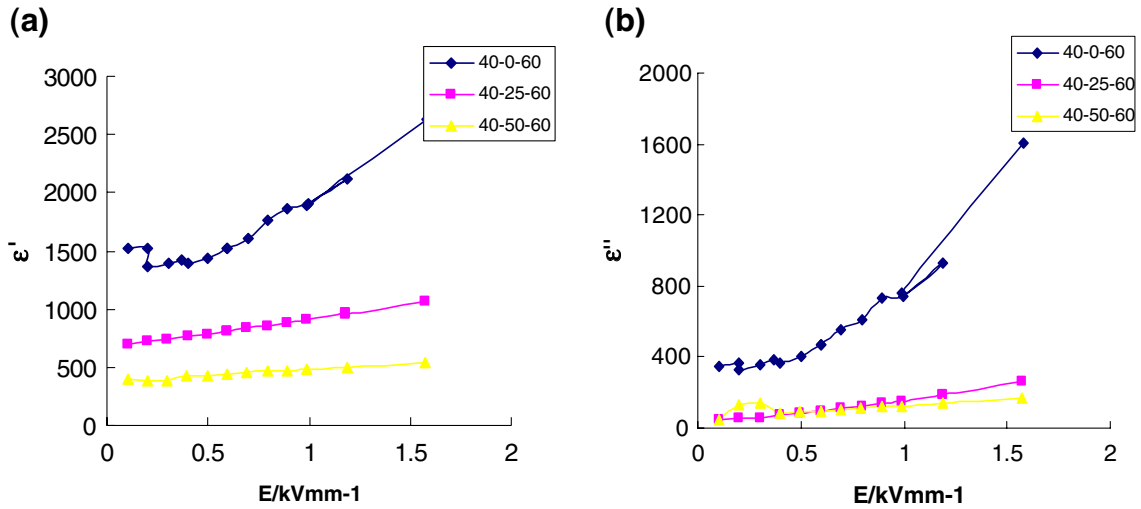

Fig. 8 (**a**) Electric field dependence of ε', (**b**) Electric field dependence of ε''

increase and pronounced broadening (indicating increases in dielectric permittivity and loss) as the electric field amplitude increased from 0.2 to 2 kV mm^{-1},as illustrated in Fig. 7. These characteristics are typical of the 'Rayleigh' loops observed at the sub switching field amplitudes in other ferroelectric ceramics [17, 18].

The main points to note are the increasing polarisation with increasing temperature for all compositions. This occurs because the coercive field reduces and so we are getting closer to the saturated P–E loop as temperature increases. For the 40–25–60 and 40–50–60 compositions, we never really approach saturation so that the polarisation values generally remain low and the loops that we observe are obtained in the sub-coercive field region. Some of the loops at high temperatures show a rounded appearance, which is a result of increasing electronic conductivity. In this case, the ferroelectric behaviour starts to become less clear because the electrical response is dominated by the conduction effects.

The hysteresis measurements reveal that the value of Residual Polarization (P_r) of the samples decreases with increase in the amount of BF. Spontaneous Polarization (P_0) also decreases in the same fashion. The coercive field (E_c) however remains almost the same for all compositions. This is expected because BF is a hardener and hence the loops get constricted [18, 19].

Early studies of dielectric nonlinearity in ferroelectric ceramics identified a 'Threshold Field' E_t, below which the dielectric properties were essentially independent of the field amplitude E_0 but beyond which both the dielectric permittivity and loss exhibited a sharp increase due to enhanced domain wall mobility or domain switching [20]. The value of E_t is often defined somewhat arbitrarily as the field amplitude at which the dielectric permittivity is

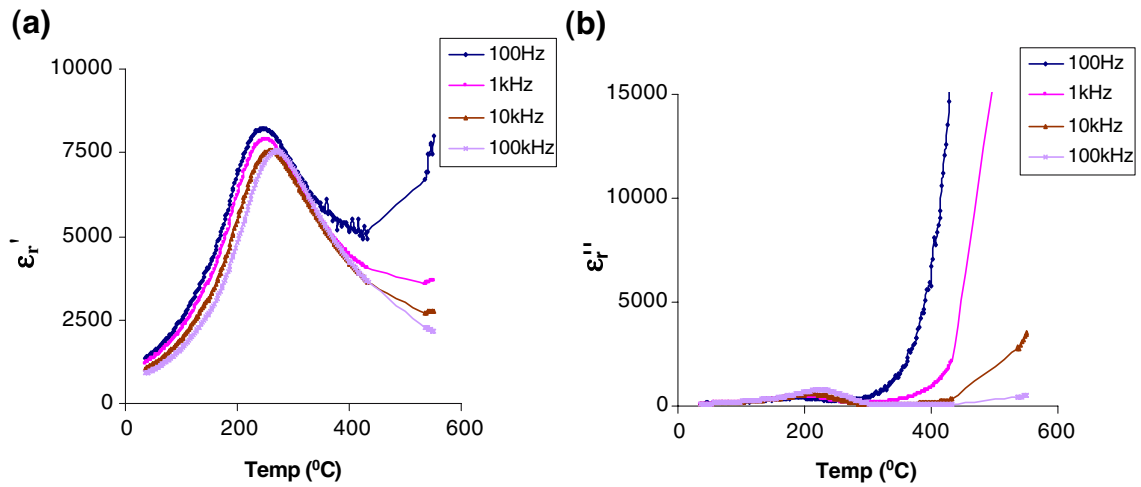

Fig. 9 (**a**) Variation of ε' with temperature; (**b**) Variation of ε'' with temperature for 40–25–60 at different frequencies for 40–25–60 at different frequencies

observed to rise by a small fraction (say 5%) above its low-field value [21]. The threshold field value was found to be much higher in hard ferroelectrics, in comparison with soft ferroelectrics, and increased significantly with ageing.

Fig. 8(a, b) shows the electric field dependence of dielectric permittivity ε' and loss ε'' in the ceramics till 2 kV mm^{-1}. It is found that, in these BF doped BMZ–PT ceramics a distinction could be made between a low field region (ε') almost constant till 0.4 kV mm^{-1}, and an intermediate Rayleigh region (ε' increasing proportionally to E_0, the applied electric field).This Rayleigh region is present till 1.2, 1.5 and 1.55 kV mm^{-1} for 40–0–60, 40–25–60 and 40–50–60 compositions at RT respectively. The slopes of the respective curves decrease with increase in the BF content in the different BMZ–PT samples. This may be due to the hardening effect which increases with increase in the BF content.

Presence of the hardener impedes the domain wall mobility or domain switching leading to which is evident from the curves for 40–0–60 and 40–25–60, 40–50–60 compositions. As the BF is introduced in the crystal lattice of BMZ–PT the cutoff low field value increases significantly.

3.4 Dielectric study

Figure 9(a, b) shows the typical results of the measurements of ε_r' and ε_r'' respectively, done at the frequencies 0.1 kHz, 1, 10 and 100 kHz for the composition 40–25–60 sintered at 1050 °C.

A frequency dispersion of the dielectric constant with respect to the temperature is observed. T_C increases with increase in frequency which shows a relaxor behavior of the material. The curve exhibits a diffused phase transition which maybe due to compositional fluctuation and structural disorderness in the system [22, 23]. There is a sudden increment in the permittivity and dielectric loss values at higher temperatures and lower frequencies. This is explained by the presence of space-charge polarization present at low frequencies and high temperatures.

4 Conclusions

A new high temperature solid-solution system BMZ–PT has been investigated. Effect of addition of BF in BMZ–PT system on the structural and ferroelectric properties has been studied in detail. Using conventional solid-state processing techniques phase pure perovskite was achieved for all the compositions. The relative density of BMZ–BF–PT was found to be >95%. At room temperature tetragonal phase was identified for BMZ–PT samples. SEM photographs reveal the uniform grain growth of all the compositions under study. With the increment in the iron content in BMZ–PT system, the residual polarization and spontaneous polarization decreased exhibiting a hardening effect of the inclusion of BF in BMZ–PT ceramics. This system shows a relaxor behavior in the dielectric-temperature characteristics.

Acknowledgements The authors wish to thank Royal Society, London, UK and Department of Science and Technology, Govt. of India for providing the financial support under INDO–UK networking scheme.

References

1. B. Jaffe, W.R. Cook, H. Jaffe, *J. Piezoelectric Ceramics* (Academic Press, New York (1971)
2. R.E. Newnham, in *J. Ferroelectric Ceramics*, ed. by N. Setter, (1992)
3. R.C. Turner, P.A. Fuierer, R.E. Newnham, T.R. Shrout, J. Appl. Acoust **41**, 299 (1994)
4. M. Naito, Ceram. Eng. Sci. Proc **8**, 1106 (1987)
5. G.A. Smolenskii, in *J. Ferroelectrics and Related Materials*, ed. by G.W. Taylor, (1984)
6. S. Zhang, D.Y. Jeong, Q. Zhang, T.R. Shrout, J. Crystal Growth **247**, 131 (2003)
7. R. Eitel, C.A. Randall, T.R. Shrout, S.E. Park, Jpn. J. Appl. Phys **41**, 2099 (2002)
8. R. Eitel, C.A. Randall, T.R. Shrout, P. Rehrig, W. Hackenberger, S.E. Park, Jpn. J. Appl. Phys **40**, 5999 (2001)
9. C.A. Randall, R. Eitel, T.R. Shrout, J. Applied Phys **93**, 9271 (2003)
10. D.I. Woodward, I.M. Reaney, R. Eitel, J. Applied Phys **94**, 3313 (2003)
11. S.A. Fedulov, Dokl. Akad. Auk. SSSR **139**, 1345 (1961)
12. S.A. Fedulov, Yu. N. Venevstev, G.U. Zhdanov et al., Soviet Phys-Crystallography **7**, 62 (1962)
13. J.R. Cheng, W.Y. Zhu, N. Li, Mater. Lett **57**, 2090 (2003)
14. D.I. Woodward, I.M. Reaney, J of Physics-Condensed Matter **16**, 8823 (2004)
15. C.A. Randall, R. Eitel, B. Jones, J of Applied Phys **95**, 3633 (2004)
16. D.A. Hall, P.J. Stevenson, T.R. Mullins, J. Brit. Cer. Proc **57**, 197 (1997)
17. D.A. Hall, P.J. Stevenson, Ferroelectrics **187**, 23 (1996)
18. D.A. Hall, P.J. Stevenson, Ferroelectrics **223**, 319 (1999)
19. U. Robels, G. Arlt, J. Appl. Phys **73**, 3454 (1993)
20. D.A. Hall, J. Mat. Sc **36**, 4575 (2001)
21. D.A. Hall, P.J. Stevenson, Proc. Br. Ceram. Soc. **57**, 197 (1997)
22. M.E. Lines, A.M. Glass, *Principles and Applications of Ferroelectrics and Related Materials* (Oxford University Press, Oxford, UK, 1978)
23. L.E. Cross, Ferroelectrics **76**, 241 (1987)